CHEMISTRY OF MATERIALS

Article

Gold Nanostar Substrates for Metal Enhanced Fluorescence through the First and Second Near-Infrared Windows

Ioannis G. Theodorou, Zaynab A. R. Jawad, Qianfan Jiang, Eric O. Aboagye, Alexandra E Porter, Mary P. Ryan, and Fang Xie

Chem. Mater., **Just Accepted Manuscript** • DOI: 10.1021/acs.chemmater.7b02313 • Publication Date (Web): 03 Aug 2017

Downloaded from http://pubs.acs.org on August 3, 2017

Just Accepted

"Just Accepted" manuscripts have been peer-reviewed and accepted for publication. They are posted online prior to technical editing, formatting for publication and author proofing. The American Chemical Society provides "Just Accepted" as a free service to the research community to expedite the dissemination of scientific material as soon as possible after acceptance. "Just Accepted" manuscripts appear in full in PDF format accompanied by an HTML abstract. "Just Accepted" manuscripts have been fully peer reviewed, but should not be considered the official version of record. They are accessible to all readers and citable by the Digital Object Identifier (DOI®). "Just Accepted" is an optional service offered to authors. Therefore, the "Just Accepted" Web site may not include all articles that will be published in the journal. After a manuscript is technically edited and formatted, it will be removed from the "Just Accepted" Web site and published as an ASAP article. Note that technical editing may introduce minor changes to the manuscript text and/or graphics which could affect content, and all legal disclaimers and ethical guidelines that apply to the journal pertain. ACS cannot be held responsible for errors or consequences arising from the use of information contained in these "Just Accepted" manuscripts.

ACS Publications

Chemistry of Materials is published by the American Chemical Society. 1155 Sixteenth Street N.W., Washington, DC 20036

Published by American Chemical Society. Copyright © American Chemical Society. However, no copyright claim is made to original U.S. Government works, or works produced by employees of any Commonwealth realm Crown government in the course of their duties.

Gold Nanostar Substrates for Metal Enhanced Fluorescence through the First and Second Near-Infrared Windows

Ioannis G. Theodorou[1], Zaynab A. R. Jawad[1], Qianfan Jiang[1], Eric O. Aboagye[2], Alexandra E. Porter[1], Mary P. Ryan[1], Fang Xie[1,]*

[1]Department of Materials and London Centre for Nanotechnology, Imperial College London, Exhibition Road, London SW7 2AZ, United Kingdom

[2]Department of Medicine, Imperial College London, Du Cane Road, London W12 0NN, United Kingdom

*E-mail: f.xie@imperial.ac.uk

Gold nanostars; self-assembled monolayers; near infrared; NIR-II; metal enhanced fluorescence; localized surface plasmon resonance; fluorescence lifetime.

Gold nanostars (AuNS) are receiving increasing attention for their potential applications in bio-nanotechnology, because of their unique optical properties related to their complex branched morphology. Their sharp features allow strong Localized Surface Plasmon Resonances (LSPRs), tunable in the near-infrared (NIR) region, and large enhancements of local electromagnetic fields. Here, the application of AuNS in metal enhanced fluorescence (MEF) in the NIR and second NIR (NIR-II) biological windows is explored for the first time. NIR/NIR-II fluorophores are incorporated on to monolayers of AuNS with tunable plasmonic responses. Over 320 times fluorescence enhancement is achieved in the NIR,

confirming that AuNS substrates are promising NIR-MEF platforms for the development of ultrasensitive biosensing applications. Using fluorescence lifetime measurements to semi-quantitatively deconvolute the excitation enhancement from emission enhancement, as well as modelling to simulate the electric field enhancement, we show that a combination of enhanced excitation and an increased radiative decay rate, accompanied by an increase to the quantum yield, contribute to the observed large enhancement. AuNS with different morphological features exhibit significantly different excitation enhancement, indicating the important role of particle morphology on the magnitude of electromagnetic field enhancement, and the resulting enhancement factor. Importantly, enhancement factors of up to 50 times are also achieved in the NIR-II region, suggesting that this system holds promise for the future development of bright probes for NIR/NIR-II biosensing and bioimaging.

Introduction

Gold nanostars (AuNS) are branched nanostructures consisting of a spherical core with several protruding spikes with sharp tips.[1-4] They have high biocompatibility and chemical stability, and unique optical properties, and therefore have attracted widespread attention for potential applications in nanomedicine. Their sharp features allow strong Localized Surface Plasmon Resonances (LSPRs), which provide the foundation for plasmon-enhanced spectroscopy,[5] and make AuNS promising tools for biological applications. Indeed, AuNS have been proposed for surface enhanced Raman scattering (SERS) substares,[6-10] as well as photothermal therapy[11, 12] and drug delivery.[13, 14] Surprisingly, attempts to apply their plasmonic properties in metal enhanced fluorescence (MEF) are lacking from the literature.

MEF is an optical process in which the near-field interaction of fluorophores with metallic nanoparticles may, under specific conditions, produce large fluorescence enhancements.[15-18] This amplification of light can be exploited to considerably increase detection sensitivity and contrast enhancement, therefore improving the performance of fluorescence-based sensing and imaging

technologies.[19] MEF is becoming important in several areas of biomedical research, including DNA[20, 21] and RNA[22] sensing, immunoassays,[23, 24] and fluorescence-based imaging.[25, 26] The magnitude of fluorescence enhancement in such applications critically depends, among several factors, on the spectral overlap between the LSPR of metal nanoparticle with the spectral properties (*i.e.* excitation and emission) of the fluorophores.[27] Therefore, AuNS, with their tunable optical properties, could be useful candidates as effective MEF agents in bio-applications, especially at biologically important wavelengths.

Two particularly relevant emission bands for bioapplications are the first (NIR; 650-900 nm) and second (NIR-II; 1.0-1.7 μm) NIR windows. Minimal light absorption from water and haemoglobin in these wavelengths, allows for high transparency when imaging soft tissue and blood.[28] Lower autofluorescence from organic molecules offers negligible background signals for biosensing,[29] while NIR imaging is non-invasive for living tissue.[29] Furthermore, reduced photon scattering allows bioimaging in the NIR-II region with higher tissue penetration.[30] However, NIR/NIR-II fluorophores exhibit much lower fluorescence emission than UV/visible dyes, which remains an obstacle in their applicability. As the design and synthesis of new photostable NIR/NIR-II fluorophores with high quantum yields has proven extremely challenging,[31] effective and scalable platforms for fluorescence enhancement in the NIR/NIR-II are highly desirable for improving detection sensitivity, and could pave the way for novel high-performance diagnostic devices.[19, 32]

To date, only a limited number of platforms allowing NIR/NIR-II fluorescence enhancement have been reported.[32-36] Recent work on NIR protein microarrays for detection of disease biomarkers has been based on porous Au films produced by dealloying.[24, 35] Similar films have also been used in one of the few attempts investigating MEF in the NIR-II region, allowing fluorescence enhancement from single walled carbon nanotubes (SWCNTs), but only by 10-fold.[37] This may be due to the fact that systematic LSPR tuning of these Au nanoporous films was not possible.[24] In our own work, arrays of Ag or Au nanotriangles with tunable optical features, obtained by nanosphere lithography, allowed fluorescence enhancement of up to two orders of magnitude, in both the NIR,[32] and NIR-II regions.[38] Bottom-up approaches for the fabrication of MEF substrates represent a lower cost alternative, that would allow the

production of arrays with flexible tuning parameters over large surface areas. Such approaches would also enable the application of anisotropic nanoparticles (NPs), including AuNS, which exhibit excellent plasmonic properties but whose potential for fluorescence enhancement in the NIR/NIR-II regions has not yet been explored.

For AuNS, the LSPR peak position and electric field enhancement largely depend on their size and shape, and are proportional to the length and aspect ratio of the spikes.[39, 40] The spike-length and aspect ratio are thought to be responsible for the observed red shift of the AuNS plasmon away from the peak of the spherical gold core.[40] Therefore, control of these morphological features allows systematic tunability of their optical properties across a wide range of the electromagnetic spectrum, reaching the NIR and NIR-II regions.[40, 41] As a result of their LSPR, the local electric field near their sharp tips, between the spikes of individual AuNS, or between the spikes of adjacent nanostars, can be enhanced by several orders of magnitude,[40, 42] holding great promise for large fluorescence enhancement. Their fabrication by wet chemical synthesis is low cost, readily scalable and can ultimately allow to synthesize multifunctional MEF agents, which induce bright NIR/NIR-II fluorescence and simultaneously carry other diagnostic or therapeutic molecules.

In the present work, fluorescent enhancement in both the NIR and NIR-II regions, using substrates based on AuNS, is reported. MEF was examined by incorporating fluorophores emitting in the NIR (two Alexa Fluor® dyes, Alexa Fluor® 750 and Alexa Fluor® 790) or NIR-II (silver sulfide quantum dots, Ag_2S QDs), on monolayers of AuNS grafted on mercaptopropyl-trimethoxysilane-coated glass slides, as illustrated schematically in Figure 1. To control the optical properties of the substrates, two different types of AuNS with LSPR positions in these spectral regions were synthesized via a surfactant-free seed-mediated method. Immobilization of fluorophore monolayers on to the arrays was attained via self-assembly of biotinylated bovine serum albumin (bBSA), followed by biotin–avidin interaction with streptavidin-functionalized fluorophores. In the NIR, significant fluorescence enhancement of more than two orders of magnitude was achieved, confirming that AuNS arrays are promising NIR-MEF platforms for the development of ultrasensitive biosensing applications, where analytes at extremely low

concentrations can be detected. Using fluorescence lifetime measurements, we showed that a combination of both enhanced excitation and an increased radiative decay rate, leading to an associated enhancement of the quantum yield, contributed to the large enhancement. For each NIR dye, emission enhancement was similar for the two types of AuNS tested, but excitation enhancement was significantly different. Electric field modelling indicated drastically enhanced local field intensities around L-AuNS compared to those of S-AuNS. These findings indicate that particle morphology largely affects the magnitude of electromagnetic field enhancement, and ultimately the total enhancement factor. Furthermore, enhancement factors of up to 46 times were also achieved in the NIR-II region, which holds great promise for the future development of bright probes for NIR-II bioimaging.

Experimental

Materials

Gold chloride trihydrate ($HAuCl_4 \cdot 3H_2O$), sodium citrate tribasic dehydrate, silver nitrate ($AgNO_3$), L-ascorbic acid (AA), hydrogen peroxide solution (H_2O_2, 30 wt. %), (3-Mercaptopropyl)trimethoxysilane (MPTMS, 95%), phosphate buffered saline (PBS, pH 7.4) and biotinylated bovine serum albumin (bBSA) were purchased from Sigma-Aldrich, UK. Glass microscope slides, hydrochloric acid (HCl, 37%), sulphuric acid (H_2SO_4, 96%), acetone and 2-propanol were obtained from VWR International, UK. Streptavidin conjugated dyes, AlexaFluor® 750 (AF750) and AlexaFluor® 790 (AF700) were purchased from Fischer Scientific. De-ionized water was purified using the Millipore Milli-Q® gradient system (>18.2 MΩ).

Methods

Synthesis and characterization of AuNS

Gold nanostars (AuNS) of two different sizes, referred to as small (S-AuNS) and large (L-AuNS) gold nanostars, were synthesized *via* a seed mediated two-step protocol. [40, 43] First, spherical citrate-stabilized

Au nanoparticle (AuNP) seeds, with average sizes of 15 nm ($AuNP_{15}$) and 50 nm ($AuNP_{50}$), were prepared by heating 100 mL of a 0.25 mM aqueous $HAuCl_4 \cdot 3H_2O$ solution in a 250 mL Erlenmeyer flask, under magnetic stirring. Once the solution reached boiling point, 1 or 0.25 mL of a 3.3% (w/v) aqueous sodium citrate solution were rapidly added, under vigorous stirring. Color started appearing in the solution after 1-3 min, and heating was continued until it became stable to a bright red color (within 10 min). The solution was then cooled in an ice bath, its volume was made up to 100 mL with Milli-Q® water, and subsequently stored at 4 ^oC.

For S-AuNS synthesis, 200 µL of $AuNP_{15}$ were added to 10 mL of 0.1 mM $HAuCl_4 \cdot 3H_2O$ with 10 µL of 1 M HCl in a 30 mL glass vial at room temperature, under moderate stirring. In the case of L-AuNS, 300 µL of $AuNP_{50}$ were added to 10 mL of 0.3 mM $HAuCl_4 \cdot 3H_2O$, containing 10 µL of 1 M HCl. Then, 150 µL of 2 mM $AgNO_3$ and 50 µL of 100 mM AA were quickly added. The color of the solution changed from faint red to blue-green as soon as AA was added, within less than 1 s, and stirring was stopped after 30 s. The extinction spectra of the solutions were measured immediately after addition of AA (t = 1 s), and monitored after up to 4 h of stirring (Supporting Information, Figure S1). Since no changes to these spectra were detected, the reaction is already complete within seconds of AA addition. Therefore, the 30 s of stirring time were selected, like previous reports,[40] as an adequate stirring time that confidently ensured that the formation of AuNS had been completed.

As-synthesized AuNPs and AuNS were characterized by optical absorption spectroscopy, using an Agilent Cary 5000 UV-Vis-NIR spectrophotometer. Extinction spectra were collected using glass cuvettes from Hellma® Analytics, and both a 100% transmittance (T) and 0% T baseline correction was applied to the data (Supporting Information, Figure S2). The 100% T baseline correction was performed using Milli-Q® water, to account for water/cuvette absorption. Transmission electron microscopy (TEM) was performed using a JEOL JEM-2100F with an accelerating voltage of 200 kV. Size distributions were measured using several TEM images and processed *via* ImageJ software (http://rsb.info.nih.gov/ij/).

Preparation of MPTMS@Glass slides

Prior to MPTMS grafting, glass microscopes slides were cut to 10 mm × 12 mm pieces and cleaned by ultrasonication in acetone, Milli-Q® water and 2-propanol, for 10 min each. The slides were dried under a N_2 stream and treated with piranha solution (3:1 v/v H_2SO_4 96%:H_2O_2 30%) for 30 min. Then, they were washed 3 times by ultrasonication in Milli-Q® water, for 3 min each. The washed slides were dried in an oven at 140 °C for 1 h, and allowed to cool to room temperature. Then, inside a glass container that had undergone the same cleaning procedure, the slides were immersed in a 5% v/v solution of MPTMS in ethanol, sealed and allowed to react for 4 h in a water bath at 40 °C. Silanization of glass surfaces is thought to take place through reaction of surface silanols with the Si-OH groups of MPTMS, leading to formation of Si(surface)-O-Si bridges.[44] The remaining Si-OH groups of MPTMS are positioned in such a way that Si-O-Si bridges can be formed between similar nearby fragments.[44] After 4 h, the MPTMS solution was discarded and the slides were washed 3 times by ultrasonication in ethanol, for 3 min each. Finally the slides were dried under a N_2 stream and cured in an oven at 100 ^oC for 15 min.

Formation of AuNS self-assembled monolayers on MPTMS@Glass slides

To form AuNS self-assembled monolayers (SAMs), the MPTMS-modified glass slides were placed in glass containers, which had been cleaned with piranha solution as described in the previous section, and immersed in solutions of freshly synthesized AuNS. The colloidal suspensions of AuNS were relatively stable up to 24 h after synthesis, under storage at 4 ^oC, with little changes observed in their extinction spectra (about 4 nm blue-shift; Figure S1, Supporting Information). However, since the method used for their synthesis was surfactant free, aggregation of the particles or blunting of their tips may occur during long-term storage.[45] Therefore, the AuNS suspensions were used for monolayer preparation only within the same day as their synthesis. The containers with the glass slides were sealed and placed on an orbital shaker (100 rpm), in the dark for 18 h. The AuNS-coated glass slides were rinsed with Milli-Q® water 3 times and gently dried under a N_2 stream. All substrates were stored under vacuum and used within 1 week of their fabrication. During this period, no changes were observed in their optical absorption spectra (Supporting Information, Figure S3), therefore we expect that minimal blunting of the AuNS tips had

occurred in the following experiments. Once grafted on the glass slides, the thiolate-gold coordinative bonds between the nanostars and MPTMS may provide some protection from reshaping.[45] However, since the top surface of the AuNS is bare, we suggest that an additional protection may be necessary for longer term storage of such substrates.

The morphology of the substrates was examined by field emission gun (FEG) scanning electron microscopy (SEM) using a LEO Gemini 1525 (Carl Zeiss Microscopy GmbH, UK). The SEM was operated in secondary electron mode at an accelerating voltage of 5 kV, using the InLens detector.

Fluorophores

The fluorophores used in this study were: (i) two commercially available streptavidin (SA)-conjugated near-infrared dyes (AF750 and AF790), and (ii) streptavidin-conjugated silver sulphide (Ag_2S) quantum dots (QDs) emitting in the second near-infrared region, synthesized *in-house*.[38]

Ag_2S QDs with an average size of 4.1 nm and an emission peak at 1200 nm were fabricated as we have previously reported.[38] They were rendered hydrophilic with a carboxylic acid group capping by ligand exchange, and conjugated with streptavidin *via* carbodiimide cross-linker chemistry.[38]

Immobilization of fluorophore–protein conjugation monolayers

The AuNS SAMs and clean glass substrates, as a control, were covered by fluorophore monolayers *via* biotin-streptavidin interaction, as previously described.[32, 38] First, to form monolayers of bBSA on the substrates, 26 μL of a 100 μg/mL bBSA solution in PBS (pH 7.2) were added to their surface, and incubated for 1 h in a humidified chamber. bBSA is known to bind, involving different binding mechanisms,[46] to both glass and Au surfaces, forming a complete monolayer. In order to be able to quantitatively compare the fluorescence intensity of fluorophore–bBSA conjugates, in the absence and presence of AuNS SAMs on glass, the amount of bound bBSA on each substrate was quantified. Therefore, following incubation, the bBSA solution was collected from each substrate. To ensure that most of unbound protein had been removed, the surface of each substrate was rinsed 3 times with 50 μL

of PBS, with each rinse being collected for bBSA quantification. The total unbound protein was quantified by measuring the absorbance of the solution at 280 nm, using disposable cuvettes with a 1 cm path length. The amount of bound bBSA on each substrate was calculated by subtraction from the total protein initially added. A straightforward version of the Lambert-Beer law for 2-dimensional materials has previously been used to determine the concentration of chromophores on surface monolayers.[44] In our experiments, however, the extinction spectra of the AuNS substrates dominated those of the overlapping AF fluorophores, making it difficult to deconvolute the two and estimate the concentration of AF dyes on the AuNS arrays. Therefore, bBSA quantification, which relied on measuring absorbance at 280 nm, was selected as an alternative method to normalize the averaged enhancement factors.

Binding of the streptavidin–conjugated fluorophores to bBSA was achieved by adding 37 µL of 25 µg/mL fluorophore solutions onto the substrate surfaces and incubating for 2 h in humidified chambers in the dark. The substrates were rinsed several times with PBS to remove unbound fluorophores and gently dried under a N_2 stream. Their fluorescence spectra were collected immediately. Clean glass substrates incubated with bBSA only, were used to establish the fluorescence background used as reference.

Fluorescence measurements and analysis

Fluorescence emission spectra of the Alexa Fluor® organic dyes were collected using a Fluorolog Tau 3 system (Horiba Scientific) with a 450 W Xenon excitation lamp. AF750 and AF790 were excited at 730 and 760 nm, respectively, using a 4 nm slit. Fluorescence emission was measured in the ranges of 760-830 nm and 785-850 nm, respectively, using a 5 nm slit. The fluorescence emission spectra of Ag_2S QDs were collected in the range of 880-1570 nm, using an NS 1 NanoSpectralyzer® (Applied NanoFluorescence, USA), with a 782 nm excitation laser and a 512 element TE-cooled InGaAs array near-IR detector. In all cases, the angle of acquisition was set at 30° for accuracy and consistency of the measurements. For all fluorophores, the fluorescence spectra were averaged over 3 individual spots on each substrate, and over 3 different substrates.

Time-correlated single-photon counting (TCSPC), which is considered as the most sensitive digital technique for determining photoluminescence lifetimes, was applied to acquire fluorescence decay curves for AF750 and AF790.[47] Lifetime data were collected using the Fluorolog Tau 3 system, equipped with a DeltaDiode™-C1 controller (Horiba Scientific). Samples were excited using the DeltaDiode™ 730L pulsed laser (Horiba Scientific), which has a peak wavelength at 730 ±10 nm, an extremely narrow 60 ps pulse width, 3.0 mW average power and a 100 MHz repetition rate. Emission was measured at 777 and 805 nm, respectively, up to 10000 counts. The fluorescence decay curves were analyzed using the DAS6 decay analysis software (Horiba Scientific) based on a multi-exponential model, which involves an iterative reconvolution process. The quality of the fits was assessed by the value of the reduced χ^2 value, and a visual inspection of the distribution of the weighted residuals and their autocorrelation function.[32]

Computational electromagnetic modelling

Calculations of the electromagnetic properties of the AuNS arrays were carried out using the finite-difference time-domain (FDTD) technique.[48] The shape of nanostars built in the simulation was based on the morphology observed in TEM images (Figure 2c, f). In brief, a 3-D total-field scheme was used with a grid resolution of 1–2 nm in each direction. The grid resolution for each case was obtained by convergence testing. The dielectric function of the nanoparticles was modelled with a Drude–Lorentz model (data provided in the Supporting Information).[49] To prevent non-physical reflections from the extremities of the FDTD workspace, perfectly matched layers (PML) were placed at the upper and lower boundaries. To simulate an infinite array of AuNS, the other boundaries had periodic boundary conditions. All FDTD calculations were carried out using the MEEP FDTD code[50] on a HP Z800 workstation with two Quad core processors and 64 GBytes of RAM.

Results and Discussion

Synthesis of AuNS with tunable morphological and optical properties

To investigate the potential of AuNS as fluorescence enhancement probes in the NIR/NIR-II windows, AuNS with LSPR maxima in these spectral regions were synthesized *via* a surfactant-free seed-mediated wet chemical synthesis,[40, 43] using 15 and 50 nm Au seeds (Figure 2a, d). A surfactant-free method was selected because the absence of polymers (*e.g.* poly(vinylpyrrolidone), PVP) or surfactants (*e.g.* cetyltrimethylammonium bromide/chloride, CTAB/CTAC), provides AuNS with high biocompatibility and ease of functionalization for the development of biological applications. Using these seeds, AuNS of two different sizes were fabricated, referred to as small (S-AuNS; Figure 2b, c) and large (L-AuNS; Figure 2e, f) AuNS. Representative TEM images (Figure 2) revealed that the particles had the typical multibranched morphology of a spherical core with several protruding spikes. The morphological properties of the AuNS, including their overall (tip-to-tip) size, core size and spike dimensions, were measured using several TEM images, and are summarized in Table 1. Apart from using different seed sizes, the morphology of AuNS was adjusted by systematically controlling other parameters of the synthesis, including the Au^{3+}, Ag^{+} and AA concentrations. This allowed to obtain AuNS with distinct differences in the number of spikes per nanoparticle and the spike sharpness, with L-AuNS exhibiting more spikes with sharper tips, whereas S-AuNS had relatively fewer spikes, with a lower aspect ratio and more rounded tips.

As anticipated, these variations in morphology allowed tunability of the optical properties of S- and L-AuNS (Figure 2g, h), which showed absorbance maxima at 718 and 1015 nm, respectively. Shoulders to the main LSPR bands also appeared at about 555 nm for S-AuNS and 850 nm for L-AuNS. AuNS are known to exhibit multiple plasmon resonances.[5] Their optical properties are highly anisotropic and strongly depend on the size of the protruding tips.[5] Using a finite-difference time-domain analysis, the plasmons of a nanostar have been shown to result from hybridization of plasmons of the core and the tips of the nanostar.[39] Using this concept, in which the core plasmons interact with the tip plasmons to form bonding and antibonding nanostar plasmons, allows to interpret the physical origin of the plasmons of such complex nanostructures.[51] Here, using AuNS with different spike aspect ratios allowed their plasmonic response to be tuned from the NIR to the NIR-II region.

Synthesis of self-assembled monolayers of AuNS grafted on glass surfaces

To fabricate MEF substrates based on AuNS, a self-assembly method was employed (Figure 1b, i-ii),[52] inspired by previous reports on the silanization of glass surfaces,[44] and their use to obtain monolayers of silver nanoparticles with antibacterial properties,[53] or AuNS for photothermal bacterial eradication.[52] The AuNS monolayers were obtained through a thiolate-gold coordinative interaction, which is moderately strong, with a homolytic strength of 40 kcal/mol.[54-56] SEM imaging showed that the surfaces of substrates fabricated with S-AuNS (Figure 3a) and L-AuNS (Figure 3d) were densely populated by particles. S-AuNS were more homogeneously distributed on the surface of glass substrates compared to L-AuNS, possibly due to an increased propensity of L-AuNS to aggregate in solution before self-assembly. However, both types of grafted AuNS maintained the shape they had in their respective colloidal solutions (Figure 3b, e). Furthermore, the resulting AuNS substrates displayed uniform colorations over their entire surface (1 cm^2; Figure 3c, f), which resembled those of the original colloidal suspensions. As previously demonstrated, the protocol employed here for the silanization of glass slides allows the formation of a smooth monolayer of MPTMS on glass, with a dense surface of reactive thiol groups.[44] As a result, thiolate-Au bonding allows self-assembled monolayers of AuNS on such slides to be obtained in a straightforward manner, simply through incubating the slides with the desired AuNS colloidal solution.

The extinction spectra of AuNS substrates were directly recorded using dry slides (Figure 3g). For both types of AuNS, a LSPR blue shift was observed when the particles were transferred from colloidal solutions to monolayers. For S-AuNS, this shift was 58 nm on average, which is close to the blue shift of about 50 nm reported in other studies when monolayers of AuNS were grafted on glass slides.[52, 57] This shift could be due to the change in the AuNS local refractive index (n), following the change of medium from water (n = 1.333) to air (n = 1.0003).[58] In fact, previous investigation of this effect by grafting AuNS on the internal wall of a glass cuvette and recording the extinction spectra using solvents of different n, showed a λ shift of 120 nm per refractive index unit.[57] For L-AuNS, the blue shift was more pronounced; similarly, another report showed that, the longer the wavelength of the colloidal AuNS LSPR peak

position, the larger the magnitude of the shift for the AuNS monolayers.[57] Moreover, for L-AuNS substrates, the LSPR peak became significantly more broadened, which could be correlated with the higher variability in interparticle distance observed for these substrates (Figure 3d). A recent work using electromagnetic computation techniques to produce predictive simulations for nanoparticle-based substrates, showed that aggregation of AuNS (20 nm core with 10 branches 15.5 nm long) in dimers and monolayers, produced widened spectral features, an increase in the magnitude of extinction, but also a slight red-shift of their extinction maximum.[59]

AuNS Substrates Afford Significant NIR Fluorescence Enhancement

The applicability of the AuNS substrates as effective MEF platforms was first investigated in the NIR region, using two commercially available NIR dyes, AlexaFluor® 750 (AF750, Abs 749 nm/Em 775 nm) and AlexaFluor® 790 (AF790, Abs 782 nm/Em 805 nm). Fluorescence enhancement was tested by immobilizing streptavidin–functionalized AlexaFluor® dye monolayers on the AuNS substrates and on bare glass substrates, as a control (Figure 1b, iii-iv). AlexaFluor® dyes were selected because they are more hydrophilic, photostable and bright, but less pH-sensitive, compared to other commercially available dyes with similar spectral properties. These features make them more suitable for biosensing applications, as well as for cell and tissue labelling.[60] Two different fluorophores were used in order to provide different degrees of spectral overlap with the LSPR properties of the AuNS (Figure 3g). Furthermore, the fluorophores represent different emission efficiencies, with quantum yields of 12% and 4% for AF750 and AF790, respectively.[32, 61]

As we have previously shown, biotin-labelled bovine serum albumin (bBSA) can act as an effective spacer between nanostructured surfaces and fluorophores.[32] bBSA is known to bind to both glass and Au surfaces; on glass, through non-covalent physisorption, while on Au surfaces, through coordinative interaction between gold and the bBSA thiol groups.[54-56] When AuNS substrates were coated with bBSA monolayers, their LSPR peak positions were red-shifted by about 6-9 nm, due to the higher refractive index of bBSA compared to air (Figure S4, Supporting Information). Similarly, a previous report showed

that the LSPR peak position of gold nanoring arrays moved to longer wavelengths by around 5 nm following bBSA binding.[62] Pre-coating the substrates with bBSA, allows binding to the streptavidin-conjugated fluorophores through avidin-biotin interaction, which is very strong ($K_a \approx 10^{15}$ M^{-1}), and leads to the formation of stable dye monolayers over the substrates.[32]

bBSA provides a spacing of ~4-8 nm between the dye molecules and the Au surface, while the streptavidin attached to the dyes, provides an additional separation distance of ~4 nm, resulting to a total spacing of ~12 nm. Fluorescence enhancement, or quenching, is largely determined by the distance between fluorophores and metal surfaces.[63] This is because the intensity of the electromagnetic field decreases with increasing distance from the metal surface, also reducing fluorescence enhancement. Numerous previous studies have been devoted to this distance-dependence of MEF. For instance, maximum fluorescence emission from PbS quantum dots coupled to AuNPs was obtained when the NPs were coated with a SiO_2 spacer of 10 nm.[64] Using Au nanorods, maximum fluorescence intensity from IRDye was observed with 17 nm spacers.[65] On the other hand, non-radiative decay processes are inversely proportional to the third power of the metal–fluorophore distance, and consequently dominate at distances <4 nm, leading to fluorescence quenching.[66, 67] In this study, using the streptavidin–biotin conjugate as a spacer, however, ensures a significantly larger spacing of ~12 nm, for which significant non-radiative decay rates are not anticipated.[32]

The averaged emission spectra of AF750 and AF790 bound to S-AuNS, L-AuNS or glass substrates, are shown in Figure 3. The averaged fluorescence enhancement factors (E_f) for each type of AuNS substrate were calculated using:

$$E_f = \frac{E_{Au/dye} - E_{glass/bBSA}}{E_{glass/dye} - E_{glass/bBSA}} \cdot \frac{bBSA_{glass}}{bBSA_{Au}} \qquad (1)$$

where $E_{Au/dye}$ and $E_{glass/dye}$ is the fluorescence intensity of the fluorophore on AuNS and bare glass substrates, respectively, $E_{glass/bBSA}$ is the background fluorescence of bBSA on bare glass substrates,

$bBSA_{glass}$ is the amount of bBSA bound on bare glass substrates and $bBSA_{Au}$ is the amount of bBSA bound on AuNS substrates. Since the adsorption efficiency of bBSA is different on glass compared to gold surfaces, the coverage of different types of substrates will vary. Quantification of the amount of bBSA adsorbed on each surface, and inclusion of the correction factor ($bBSA_{glass}/bBSA_{Au}$) allowed us to adjust the enhancement factors for these differences. The calculated averaged fluorescence enhancement factors (E_f), which are in effect the useful parameter for applications such as biosensing, are summarized in Table 2.

As shown in Table 2, all the fluorophores exhibited significantly enhanced fluorescence, of up to 320 times, on AuNS substrates. MEF is an intricate coupling process between fluorescent molecules and metal nanostructures, which can occur *via*: (i) excitation enhancement, whereby local enhancements of the electric field induced by the LSPR of metal nanoparticles, can result to higher excitation rates of the fluorophores, or (ii) emission enhancement, which refers to the modification of radiative and non-radiative decay rates of nearby fluorophores by metal nanoparticles, leading to a change in their lifetime and quantum yield.[32, 63] Several parameters may influence the fluorescence enhancement factors of metal nanoparticles, including particle size, shape, interparticle separation, the surrounding dielectric medium, as well as the particle arrangement geometry and the separation distance with fluorophores.[35, 63, 66] Another critical factor determining the magnitude of MEF, is the spectral overlap of the LSPR of metal nanoparticles with the spectral properties of the fluorophore.

In the present work, the highest fluorescence enhancement was measured for AF750 on L-AuNS substrates, resulting to more than two orders of magnitude higher fluorescence compared to bare glass. The enhancement factors were higher for AF750 than AF790, on both types of AuNS substrates, which may be attributed to the localization of the excitation/emission properties of AF750 in closer proximity to the LSPR of the substrates. For both fluorophores used, fluorescence enhancement was significantly larger with L-AuNS substrates, compared to S-AuNS substrates. On the one hand, this observation may be due to the higher degree of spectral overlap between the LSPR of the L-AuNS substrates with the PL excitation and emission spectra of the AF dyes (Figure 2g), which is crucial to obtaining the maximum

fluorescence enhancement. On the other hand, these findings may imply higher enhancement of the local electromagnetic fields by L-AuNS, leading to an increased excitation rate of the fluorophores. For AuNS, electric field enhancement is localized at the tip of their branches,[68, 69] and has been shown to depend on the morphology of the spikes, with sharper tips producing larger enhancements.[70] In sensing applications, the ability to predict and adjust the enhancement factor of plasmonic substrates is crucial for optimizing the quantitative detection of different analytes in their respective concentration ranges, by tuning the sensitivity and dynamic range of the array. Therefore, AuNS, which can be fabricated with tunable morphologies and optical properties, consequently providing tailored enhancement factors, may be a significant step forward in the application of MEF in biomedical applications. To provide further insights into the mechanism of fluorescence enhancement from AuNS, we proceeded to perform fluorescence *lifetime* measurements and electric field modelling.

Exploring the Origins of NIR-MEF from AuNS Substrates

The fluorescence decay curves of AF750 and AF790 on the two types of AuNS substrates, and control bare glass substrates, are shown in Figure 4. Fluorescence lifetime data can be evaluated using a single exponential (SE) model, suitable for single fluorophores in homogeneous environments, or a multiexponential (ME) model, which describes the fractional contribution of decay times from different components in a sample mixture.[71] Here, satisfactory fitting of our data required a model with three decay times, τ_1, τ_2 and τ_3, from which the average decay time was calculated using the weighting a_1, a_2 and a_3 for each of the decay components:

$$I(t) = a_1 e^{-\frac{t}{\tau_1}} + a_2 e^{-\frac{t}{\tau_2}} + a_3 e^{-\frac{t}{\tau_3}} \qquad (2)$$

The results of this fitting are summarized in Table 3. The goodness of fit parameter (χ_R^2) was obtained by fitting experimentally measured parameters to calculated values, through a nonlinear least-squares

deconvolution process.[71] The average fluorescence lifetimes (τ) of AF750 and AF790 monolayers on glass, were found to be 0.72 ns and 0.55 ns, respectively, in accordance to the values provided by the manufacturer and measured in our previous work,[32, 61] and were reduced for both fluorophores, on both types of AuNS substrates tested.

Much of the recent literature in fluorescence has established a widely accepted semi-empirical model for the plasmonic enhancement effects associated with fluorophores.[72] For isolated fluorophores, in the absence of metal nanoparticles or any quenching interactions, their emission can be described in terms of their quantum yield (Q_0) and lifetime (τ_0). Q_0 is defined as the ratio of radiative relaxation rate (Γ_0) to the total relaxation rate (Γ_0+k_{nr}), where k_{nr} is the non-radiative decay rate:

$$Q_0 = \frac{\Gamma_0}{\Gamma_0+k_{nr}} \qquad (3)$$

The lifetime is given by the inverse of the total decay rate:

$$\tau_0 = \frac{1}{\Gamma_0+k_{nr}} \qquad (4)$$

For fluorophores close to metal nanoparticles, enhancement of the near field can increase the energy absorbed by the fluorophore. Additionally, electromagnetic coupling between the fluorophore and the LSPR of the nanoparticles, increases the radiative decay rate of the fluorophore by a rate Γ_m. Therefore, the modified quantum yield (Q_m) and lifetime (τ_m) are:

$$Q_m = \frac{\Gamma_m+\Gamma_0}{\Gamma_m+\Gamma_0+\Gamma_{m,abs}+k_{nr}} \qquad (5)$$

$$\tau_m = \frac{1}{\Gamma_m+\Gamma_0+\Gamma_{m,abs}+k_{nr}} \qquad (6)$$

$\Gamma_{m,abs}$ is the additional non-radiative decay rate, whose effectiveness falls off rapidly with separation distance, and thus the modified quantum yield tends back to its original value at far enough separation. As the separation distance becomes very small (<5 nm), the fluorophore is quenched by the metal nanoparticle, until complete quenching occurs. In our experiments, the spacing between fluorophores and AuNS provided by the streptavidin–biotin conjugate (~12 nm), prevents a significant increase in the non-radiative decay rate. Therefore, the non-radiative decay rates for AF750 and AF790 on both glass and AuNS substrates can be considered equal, meaning that the term $\Gamma_{m,abs}$ can be neglected.

Using the measured fluorescence lifetimes of AF750 and AF790 on glass, the unmodified quantum yields of AF750 (12%) and AF790 (4%),[32, 61] and equations (3)-(6), we calculated the modified quantum yield for each AuNS substrate, and thus the emission enhancement factor, defined as $E_{em} = Q_m/Q_0$. The excitation enhancement factor was then calculated using: $E_{ex} = E_f/E_{em}$. The excitation (E_{ex}) and emission (E_{em}) enhancement factors for each substrate are shown in Table 4.

The results of the fluorescence lifetime study, show that for each fluorophore, the lifetime followed a reverse trend with the total fluorescence enhancement factor, with shorter lifetimes correlating to higher enhancement factors. The radiative decay rates of both fluorophores increased on AuNS substrates, with a resulting increase to the fluorophores' quantum yields. However, significantly higher increases to the quantum yield were observed for AF790, which had a lower unmodified quantum yield, compared to AF750. The high quantum yield of 74% measured for AF790 on L-AuNS substrates shows that AuNS can be used as plasmonic enhancement platforms that increase the brightness of NIR dyes to levels comparable to those of visible dyes.

As shown in Table 4, it was possible to semi-quantitatively to deconvolute excitation enhancement from emission enhancement, the two main mechanisms for the observed fluorescence enhancement. The observed emission enhancement indicates that both fluorophores coupled to the LSPR generated by the AuNS. Interestingly, for each dye, the extent of emission enhancement was similar for both types of AuNS substrates. However, for both dyes, excitation enhancement was significantly higher with L-AuNS

compared to S-AuNS. Since excitation enhancement is related to the electric field experienced by the fluorophore, this observation implies that *the electromagnetic field enhancement in L-AuNS substrates is much larger than S-AuNS.*

To provide further insights, 3D finite-difference time-domain (FDTD) modelling was carried out to simulate the electric field enhancement at the excitation wavelength of 790 nm (Figure 6). The simulated field distribution around L-AuNS indicates drastically enhanced local field intensities compared to those of S-AuNS, in agreement with our experimental observations. More importantly, although our fluorescence measurements were averaged over comparatively large surface areas, significant excitation enhancement actually occurs at the tip regions of AuNS with strong electric near fields, which tend to be strongly confined, as shown in Figure 6. In summary, our experimental data together with the simulations, demonstrate that L-AuNS provide strong field enhancement that is significantly larger than that of S-AuNS. Similar to our findings, previous work revealed that for AuNS, the hot spots were localized around the sharp edges of the spikes, and provided large field enhancements.[68, 69] Electric field enhancement in AuNS have been attributed to both plasmonic contributions and the lightning rod effect.[73] Consequently, AuNS with sharper spikes produce larger enhancements.[70] In addition, electric field enhancements have been shown to grow with increasing number of branches.[69] In arrays of nanoparticles, E-field enhancements are also known to highly depend on gap size, with narrower gap sizes leading to plasmon coupling and significantly enhancing the field close to the metal nanoparticle.[67] For AuNS assemblies on glass substrates, the field enhancement from AuNS-AuNS coupling has previously been shown to decrease exponentially with increasing interparticle distance, as is typically observed for near-field interactions in nanoparticle assemblies.[74]

In summary, our analysis suggests that tuning the total fluorescent enhancement essentially depends on controlling the excitation enhancement, and illustrates the significant impact of nanotopography on fluorescence enhancement. Our findings clearly demonstrate that AuNS substrates are effective MEF platforms for the enhancement of light from NIR dyes, leading to brightness comparable to that of visible dyes.

AuNS Substrates Allow Fluorescence Enhancement in the NIR-II Region

Finally, the potential to use AuNS to enhance fluorescence in the NIR-II wavelength range was tested using Ag_2S QDs. Detection in this NIR-II window is particularly intriguing, because of its non-invasive character for living tissues, reduced autofluorescence and deep tissue penetration.[1] Ag_2S QDs were selected as the NIR-II fluorophore to test because, among the limited number of probes reported to date, these benefit from high biocompatibility and tunability of their emission to discrete wavelengths.[38, 75] However, their low fluorescence quantum yield (<10%), limits their exploitation in imaging applications. The Ag_2S QDs (4.1 nm in diameter) were synthesized *in-house*, had no discrete absorption features, and a fluorescence emission peak at 1200 nm (Figure 3g), as previously described in detail.[38] The Ag_2S QDs were functionalized with streptavidin, allowing QD monolayers on the AuNS substrates to be formed in an identical manner as the organic NIR fluorophores. The fluorescence emission spectra of Ag_2S QD monolayers on S- and L-AuNS substrates, as well as bBSA-coated glass slides for background control, are shown in Figure 7. The Ag_2S QDs exhibited enhanced fluorescence on both types of AuNS substrates, and the averaged fluorescence enhancement factors, shown in Table 2, were calculated using Equation (1). The higher enhancement factor measured for L-AuNS compared to S-AuNS, may be in part due to the much better degree of spectral overlap between the LSPR of L-AuNS with the emission spectra of the QDs, which is a critical factor for the magnitude of fluorescence enhancement. The considerable fluorescent enhancement of up to 46 times measured, shows that AuNS can also be applied for the enhancement of light from NIR-II dyes. These findings are promising for the development of bright probes for bioimaging in the NIR-II window, with significantly improved detection sensitivity and contrast enhancement.

Conclusions

In summary, the present work shows that AuNS arrays are effective MEF platforms in the NIR and NIR-II regions. In the NIR, significant fluorescence enhancement of up to 320 times is demonstrated,

confirming that AuNS arrays are promising NIR-MEF platforms for the development of ultrasensitive biosensing applications, able to detect ultralow concentrations of analytes. Fluorescence lifetime measurements indicate that a combination of enhanced excitation and an increased radiative decay rate, resulting to an enhancement of the quantum yield, contribute to the large enhancement. Our findings also suggest that particle morphology may largely affect the magnitude of electromagnetic field enhancement, and ultimately the total enhancement factor. Finally, MEF in the NIR-II region using AuNS is demonstrated, with enhancement factors of up to 50 times, paving the way for the development of bright probes for NIR-II bioimaging.

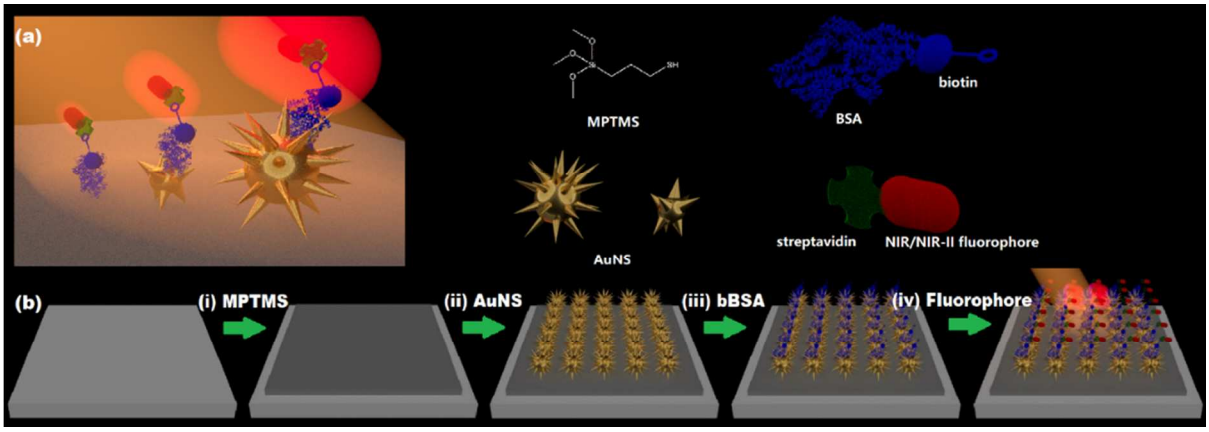


Figure 1. (a) Substrates based on spiky gold nanostars (AuNS) are efficient platforms for metal enhanced fluorescence (MEF) in the near-infrared (NIR) and second near-infrared (NIR-II) regions, allowing up to two orders of magnitude fluorescence enhancement. The enhancement factors can be tuned through control of the nanostar morphology. (b) Schematic workflow of MEF on AuNS substrates: glass slides are coated with mercaptopropyl-trimethoxysilane (MPTMS; i) and used for the fabrication of AuNS monolayers through thiolate-gold coordinative bonding (ii). Deposition of a self-assembled monolayer of biotinylated bovine serum albumin (bBSA; iii) allows immobilization of fluorophore monolayers onto the substrates (iv), through biotin–avidin interaction with the streptavidin-functionalized fluorophores.

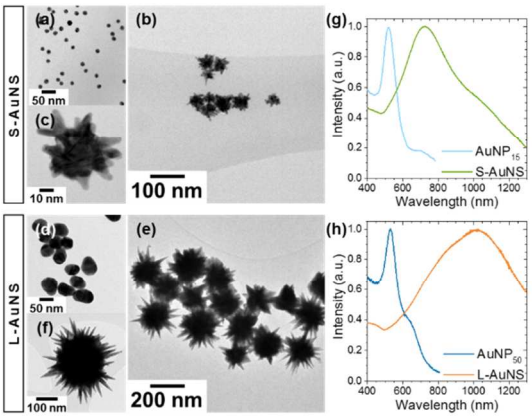


Figure 2. (a-f) Transmission electron microscopy (TEM) images of 15 nm ($AuNP_{15}$; a; σ = 3 nm) and 50 nm ($AuNP_{15}$; d; σ = 13 nm) citrate-stabilized gold nanoparticles (AuNPs), used for the surfactant-free seed-mediated synthesis of "small" (S-AuNS; b, c) and "large" (L-AuNS; e, f) gold nanostars (AuNS). (g, h) Normalized extinction spectra of AuNP seeds and the corresponding AuNS.

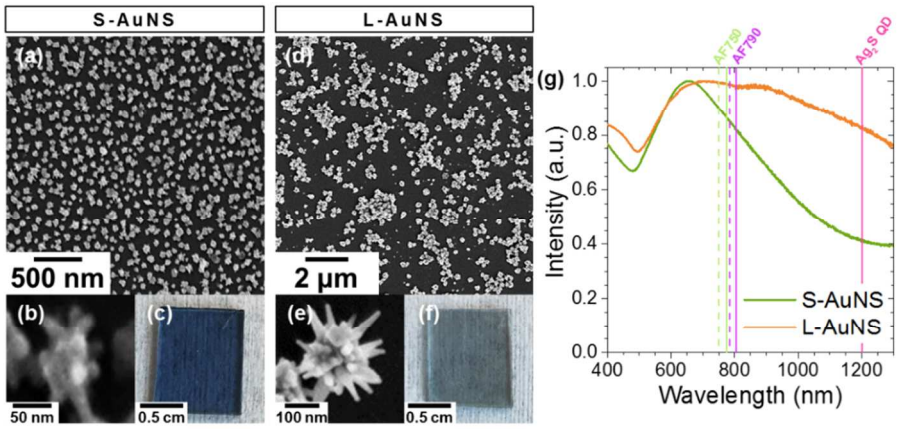


Figure 3. Low magnification (a, d) and high magnification (b, e) scanning electron microscopy (SEM) images, and photographs (c, f) of substrates fabricated through the self-assembly of S-AuNS (a-c) and L-AuNS (d-f) on MPTMS-coated glass slides. (g) Normalized extinction spectra of the S- and L-AuNS substrates. The dashed straight lines represent the excitation maxima of Alexa Fluor® 750 (AF750) and Alexa Fluor® 790 (AF790), while the solid straight lines signify the emission maxima of AF750, AF790 and silver sulfide quantum dots (Ag_2S QDs).

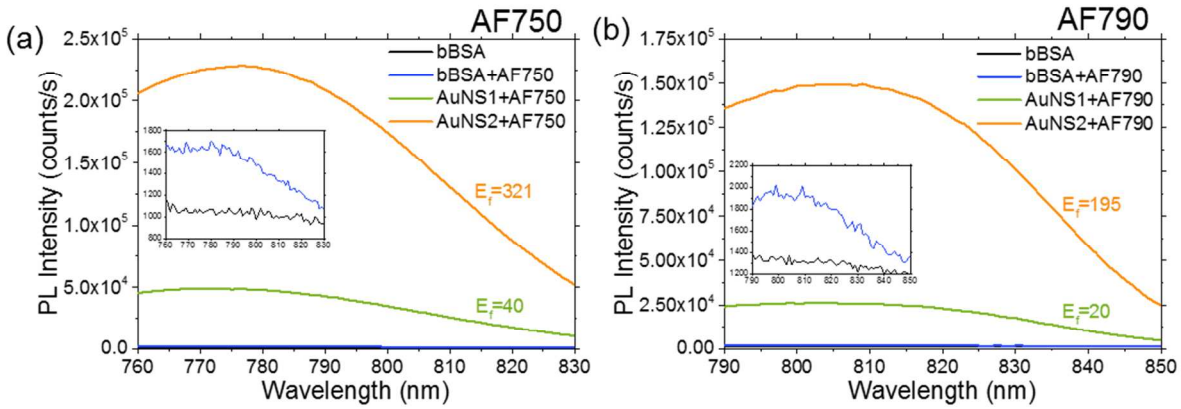


Figure 4. Photoluminescence (PL) emission spectra of monolayers of streptavidin-conjugated AF750 (a) and AF790 (b), formed on biotinylated bovine serum albumin (bBSA)-coated glass slides and S- or L-AuNS substrates. The insets show the PL emission of AF750 and AF790 on bBSA-coated glass compared to bare (*i.e.* with no fluorophore) bBSA-coated glass slides, used for background correction.

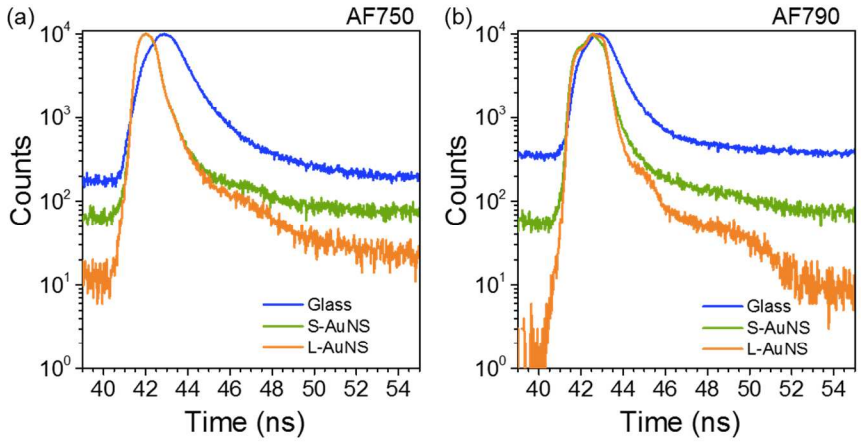


Figure 5. Fluorescence lifetime spectra of streptavidin-conjugated AF750 (a) and AF790 (b) monolayers, immobilized on S- and L-AuNS substrates, and on glass surfaces as a control.

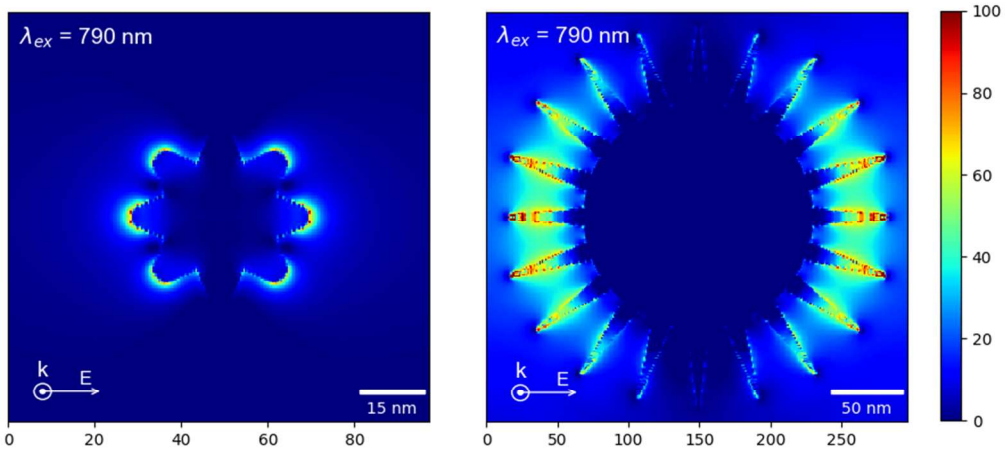


Figure 6: E-field enhancement calculated with 3D finite-difference time-domain (FDTD) modelling for S-AuNS (a) and L-AuNS (b). The figure indicates a cross-sectional E-field mapping through the center of gold nanostars with a 790 nm incident wave, of which **k**, the incident wave vector, is perpendicular to the plotting plane and **E** is the electric field polarization in the simulation.

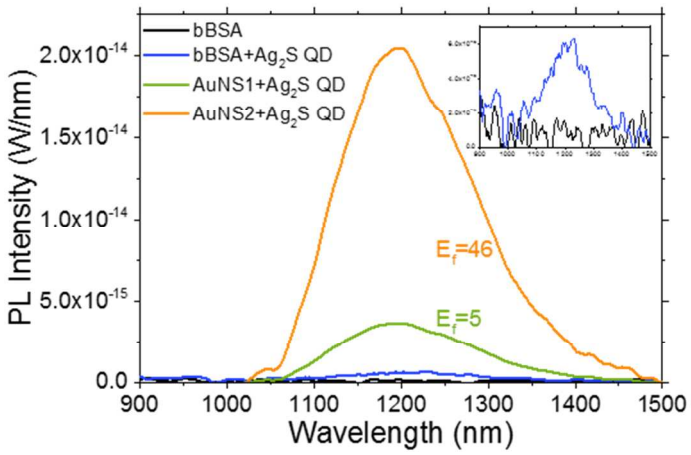


Figure 7. PL emission spectra of monolayers of streptavidin-conjugated Ag_2S QDs formed on bBSA-coated glass slides and S- or L-AuNS substrates. Bare (*i.e.* with no fluorophore) bBSA-coated glass slides were used for background correction.

Table 1. Morphological characteristics and extinction peak positions of S-AuNS and L-AuNS obtained through seed-mediated synthesis.

	Number of spikes	Size (nm)	Core Size (nm)	Spike length (nm)	Spike width (nm)	Spike Aspect Ratio	λ_{max} (nm)
S-AuNS	8-16	47 ± 17	27 ± 7	10 ± 6	7 ± 3	1.4	718 nm
L-AuNS	14-26	214 ± 90	132 ± 34	60 ± 52	13 ± 12	4.6	1015 nm

Table 2. Average fluorescence enhancement factors (E_f) for monolayers of streptavidin-conjugated AF750, AF790 and Ag_2S QDs, immobilized on S- and L-AuNS substrates.

Fluorophore	Substrate	Enhancement Factor (E_f)
AF750	S-AuNS	40
	L-AuNS	321
AF790	S-AuNS	20
	L-AuNS	195
Ag_2S QDs	S-AuNS	5
	L-AuNS	46

Table 3. Multi-exponential analysis of intensity decay of AF750 and AF790 monolayers on glass substrates and S- or L-AuNS substrates, showing the weighting fractions (a_1, a_2, a_3), the observed lifetimes (τ_1, τ_2 and τ_3), the intensity-weighted lifetime (τ), and the goodness of fit parameter (χ_R^2) .

Fluorophore	Substrate	a_1	a_2	a_3	τ_1 (ns)	τ_2 (ns)	τ_3 (ns)	τ (ns)	χ_R^2
AF750	Glass	85.9%	14.1%	-	0.55	1.8	-	0.72	1.300
	S-AuNS	60.2%	28.3%	11.5%	0.34	0.53	2.4	0.63	1.754
	L-AuNS	47.3%	45.1%	7.6%	0.16	0.49	2.9	0.52	1.657
AF790	Glass	60.7%	39.3%	-	0.31	0.92	-	0.55	1.577
	S-AuNS	95.0%	3.2%	1.9%	0.03	0.64	7.3	0.18	1.715
	L-AuNS	93.6%	5.1%	1.4%	0.02	0.63	6.6	0.15	1.859

Table 4: Calculated values of modified quantum yield (Q_m), total enhancement factor (E_f), emission enhancement factor (E_{em}) and excitation enhancement factor (E_{ex}) of AF750 (Em 775 nm) and AF790 (Em 805 nm) on S- and L-AuNS substrates.

Fluorophore	Substrate	Q_m	E_f	E_{em}	E_{ex}
AF750	S-AuNS	0.23	40	1.9	20.9
	L-AuNS	0.36	321	3.0	107.0
AF790	S-AuNS	0.68	20	17.0	1.1
	L-AuNS	0.74	195	18.6	10.5

ASSOCIATED CONTENT

Supporting Information. Supplementary figures and parameters used in FDTD calculations

AUTHOR INFORMATION

Corresponding Author

* E-mail: f.xie@imperial.ac.uk

Author Contributions

All authors have given approval to the final version of the manuscript.

ACKNOWLEDGMENT

I.G.T. and F.X are supported by a British Council Newton Grant (#216239013).

REFERENCES

1. Guerrero-Martínez, A.; Barbosa, S.; Pastoriza-Santos, I.; Liz-Marzán, L. M. Nanostars shine bright for you: Colloidal synthesis, properties and applications of branched metallic nanoparticles. *Curr. Opin. Colloid Interface Sci.* **2011**, 16, 118-127.

2. Burt, J. L.; Elechiguerra, J. L.; Reyes-Gasga, J.; Martin Montejano-Carrizales, J.; Jose-Yacaman, M. Beyond Archimedean solids: Star polyhedral gold nanocrystals. *J. Cryst. Growth* **2005**, 285, 681-691.

3. Jiang, L.; Tang, Y.; Liow, C.; Wu, J.; Sun, Y.; Jiang, Y.; Dong, Z.; Li, S.; Dravid, V. P.; Chen, X. Synthesis of Fivefold Stellate Polyhedral Gold Nanoparticles with {110}-Facets via a Seed-Mediated Growth Method. *Small* **2013**, 9, 705-710.

4. Cabrera-Trujillo, J. M.; Montejano-Carrizales, J. M.; Rodríguez-López, J. L.; Zhang, W.; Velázquez-Salazar, J. J.; José-Yacamán, M. Nucleation and Growth of Stellated Gold Clusters: Experimental Synthesis and Theoretical Study. *J. Phys. Chem. C* **2010**, 114, 21051-21060.

5. Nehl, C. L.; Liao, H.; Hafner, J. H. Optical Properties of Star-Shaped Gold Nanoparticles. *Nano Lett.* **2006**, 6, 683-688.

6. Niu, W.; Chua, Y. A.; Zhang, W.; Huang, H.; Lu, X. Highly Symmetric Gold Nanostars: Crystallographic Control and Surface-Enhanced Raman Scattering Property. *J. Am. Chem. Soc.* **2015**, 137, 10460-10463.

7. Indrasekara, A. S.; Meyers, S.; Shubeita, S.; Feldman, L. C.; Gustafsson, T.; Fabris, L. Gold nanostar substrates for SERS-based chemical sensing in the femtomolar regime. *Nanoscale* **2014**, 6, 8891-8899.

8. Fales, A. M.; Yuan, H.; Vo-Dinh, T. Development of Hybrid Silver-Coated Gold Nanostars for Nonaggregated Surface-Enhanced Raman Scattering. *J. Phys. Chem. C* **2014**, 118, 3708-3715.

9. Schutz, M.; Steinigeweg, D.; Salehi, M.; Kompe, K.; Schlucker, S. Hydrophilically stabilized gold nanostars as SERS labels for tissue imaging of the tumor suppressor p63 by immuno-SERS microscopy. *Chem. Commun.* **2011**, 47, 4216-4218.

10. Li, M.; Kang, J. W.; Dasari, R. R.; Barman, I. Shedding Light on the Extinction-Enhancement Duality in Gold Nanostar-Enhanced Raman Spectroscopy. *Angew. Chem.* **2014**, 126, 14339-14343.

11. Cheng, L.-C.; Huang, J.-H.; Chen, H. M.; Lai, T.-C.; Yang, K.-Y.; Liu, R.-S.; Hsiao, M.; Chen, C.-H.; Her, L.-J.; Tsai, D. P. Seedless, silver-induced synthesis of star-shaped gold/silver bimetallic nanoparticles as high efficiency photothermal therapy reagent. *J. Mater. Chem.* **2012**, 22, 2244-2253.

12. Yuan, H.; Fales, A. M.; Vo-Dinh, T. TAT Peptide-Functionalized Gold Nanostars: Enhanced Intracellular Delivery and Efficient NIR Photothermal Therapy Using Ultralow Irradiance. *J. Am. Chem. Soc.* **2012**, 134, 11358-11361.

13. Dam, D. H. M.; Lee, R. C.; Odom, T. W. Improved in Vitro Efficacy of Gold Nanoconstructs by Increased Loading of G-quadruplex Aptamer. *Nano Lett.* **2014**, 14, 2843-2848.

14. Dam, D. H. M.; Lee, J. H.; Sisco, P. N.; Co, D. T.; Zhang, M.; Wasielewski, M. R.; Odom, T. W. Direct Observation of Nanoparticle–Cancer Cell Nucleus Interactions. *ACS Nano* **2012**, 6, 3318-3326.

15. Anger, P.; Bharadwaj, P.; Novotny, L. Enhancement and Quenching of Single-Molecule Fluorescence. *Phys. Rev. Lett.* **2006**, 96, 113002.

16. Geddes, C. D.; Lakowicz, J. R. Editorial: Metal-Enhanced Fluorescence. *J. Fluoresc.* **2002**, 12, 121-129.

17. Pompa, P. P.; MartiradonnaL; Torre, A. D.; Sala, F. D.; MannaL; De Vittorio, M.; CalabiF; CingolaniR; RinaldiR. Metal-enhanced fluorescence of colloidal nanocrystals with nanoscale control. *Nat. Nanotechnol.* **2006**, 1, 126-130.

18. Deng, W.; Goldys, E. M. Plasmonic Approach to Enhanced Fluorescence for Applications in Biotechnology and the Life Sciences. *Langmuir* **2012**, 28, 10152-10163.

19. Darvill, D.; Centeno, A.; Xie, F. Plasmonic fluorescence enhancement by metal nanostructures: shaping the future of bionanotechnology. *Phys. Chem. Chem. Phys.* **2013**, 15, 15709-15726.

20. Cheng, Y.; Stakenborg, T.; Van Dorpe, P.; Lagae, L.; Wang, M.; Chen, H.; Borghs, G. Fluorescence Near Gold Nanoparticles for DNA Sensing. *Anal. Chem.* **2011**, 83, 1307-1314.

21. Wang, Y.; Liu, B.; Mikhailovsky, A.; Bazan, G. C. Conjugated Polyelectrolyte–Metal Nanoparticle Platforms for Optically Amplified DNA Detection. *Adv Mater.* **2010**, 22, 656-659.

22. Aslan, K.; Huang, J.; Wilson, G. M.; Geddes, C. D. Metal-Enhanced Fluorescence-Based RNA Sensing. *J. Am. Chem. Soc.* **2006**, 128, 4206-4207.

23. Szmacinski, H.; Murtaza, Z.; Lakowicz, J. R. Time-Resolved Fluorometric Method for One-Step Immunoassays Using Plasmonic Nanostructures. *J. Phys. Chem. C* **2010**, 114, 7236-7241.

24. Tabakman, S. M.; Lau, L.; Robinson, J. T.; Price, J.; Sherlock, S. P.; Wang, H.; Zhang, B.; Chen, Z.; Tangsombatvisit, S.; Jarrell, J. A.; Utz, P. J.; Dai, H. Plasmonic substrates for multiplexed protein microarrays with femtomolar sensitivity and broad dynamic range. *Nat. Commun.* **2011**, 2, 466.

25. Zhang, J.; Fu, Y.; Lakowicz, J. R. Fluorescent Metal Nanoshells: Lifetime-Tunable Molecular Probes in Fluorescent Cell Imaging. *J. Phys. Chem. C* **2011**, 115, 7255-7260.

26. Saha, A.; Basiruddin, S. K.; Sarkar, R.; Pradhan, N.; Jana, N. R. Functionalized Plasmonic−Fluorescent Nanoparticles for Imaging and Detection. *J. Phys. Chem. C* **2009**, 113, 18492-18498.

27. Aslan, K.; Lakowicz, J. R.; Geddes, C. D. Plasmon light scattering in biology and medicine: new sensing approaches, visions and perspectives. *Curr. Opin. Chem. Biol.* **2005**, 9, 538-544.

28. Weissleder, R. A clearer vision for in vivo imaging. *Nat. Biotechnol.* **2001**, 19, 316-317.

29. Hilderbrand, S. A.; Weissleder, R. Near-infrared fluorescence: application to in vivo molecular imaging. *Curr. Opin. Chem. Biol.* **2010**, 14, 71-79.

30. Hong, G.; Diao, S.; Chang, J.; Antaris, A. L.; Chen, C.; Zhang, B.; Zhao, S.; Atochin, D. N.; Huang, P. L.; Andreasson, K. I.; Kuo, C. J.; Dai, H. Through-skull fluorescence imaging of the brain in a new near-infrared window. *Nat. Photonics* **2014**, 8, 723-730.

31. Licha, K.; Riefke, B.; Ntziachristos, V.; Becker, A.; Chance, B.; Semmler, W. Hydrophilic Cyanine Dyes as Contrast Agents for Near-infrared Tumor Imaging: Synthesis, Photophysical Properties and Spectroscopic In vivo Characterization. *Photochem. Photobiol.* **2000**, 72, 392-398.

32. Xie, F.; Pang, J. S.; Centeno, A.; Ryan, M. P.; Riley, D. J.; Alford, N. M. Nanoscale control of Ag nanostructures for plasmonic fluorescence enhancement of near-infrared dyes. *Nano Res.* **2013**, 6, 496-510.

33. Sugawa, K.; Tamura, T.; Tahara, H.; Yamaguchi, D.; Akiyama, T.; Otsuki, J.; Kusaka, Y.; Fukuda, N.; Ushijima, H. Metal-Enhanced Fluorescence Platforms Based on Plasmonic Ordered Copper Arrays: Wavelength Dependence of Quenching and Enhancement Effects. *ACS Nano* **2013**, 7, 9997-10010.

34. Camposeo, A.; Persano, L.; Manco, R.; Wang, Y.; Del Carro, P.; Zhang, C.; Li, Z.-Y.; Pisignano, D.; Xia, Y. Metal-Enhanced Near-Infrared Fluorescence by Micropatterned Gold Nanocages. *ACS Nano* **2015**, 9, 10047-10054.

35. Bardhan, R.; Grady, N. K.; Cole, J. R.; Joshi, A.; Halas, N. J. Fluorescence Enhancement by Au Nanostructures: Nanoshells and Nanorods. *ACS Nano* **2009**, 3, 744-752.

36. Ayala-Orozco, C.; Liu, J. G.; Knight, M. W.; Wang, Y.; Day, J. K.; Nordlander, P.; Halas, N. J. Fluorescence enhancement of molecules inside a gold nanomatryoshka. *Nano Lett.* **2014**, 14, 2926-2933.

37. Hong, G.; Tabakman, S. M.; Welsher, K.; Wang, H.; Wang, X.; Dai, H. Metal-Enhanced Fluorescence of Carbon Nanotubes. *J. Am. Chem. Soc.* **2010**, 132, 15920-15923.

38. Theodorou, I. G.; Jawad, Z. A. R.; Qin, H.; Aboagye, E. O.; Porter, A. E.; Ryan, M. P.; Xie, F. Significant metal enhanced fluorescence of Ag_2S quantum dots in the second near-infrared window. *Nanoscale* **2016**, 8, 12869-12873.

39. Hao, F.; Nehl, C. L.; Hafner, J. H.; Nordlander, P. Plasmon Resonances of a Gold Nanostar. *Nano Lett.* **2007**, 7, 729-732.

40. Yuan, H.; Khoury, C. G.; Hwang, H.; Wilson, C. M.; Grant, G. A.; Vo-Dinh, T. Gold nanostars: surfactant-free synthesis, 3D modelling, and two-photon photoluminescence imaging. *Nanotechnology* **2012**, 23, 075102.

41. Pallavicini, P.; Dona, A.; Casu, A.; Chirico, G.; Collini, M.; Dacarro, G.; Falqui, A.; Milanese, C.; Sironi, L.; Taglietti, A. Triton X-100 for three-plasmon gold nanostars with two photothermally active NIR (near IR) and SWIR (short-wavelength IR) channels. *Chem. Commun.* **2013**, 49, 6265-6267.

42. Lee, J.; Hua, B.; Park, S.; Ha, M.; Lee, Y.; Fan, Z.; Ko, H. Tailoring surface plasmons of high-density gold nanostar assemblies on metal films for surface-enhanced Raman spectroscopy. *Nanoscale* **2014**, 6, 616-623.

43. Khlebtsov, B.; Panfilova, E.; Khanadeev, V.; Khlebtsov, N. Improved size-tunable synthesis and SERS properties of Au nanostars. *J. Nanopart. Res.* **2014**, 16, 1-12.

44. Pallavicini, P.; Dacarro, G.; Galli, M.; Patrini, M. Spectroscopic evaluation of surface functionalization efficiency in the preparation of mercaptopropyltrimethoxysilane self-assembled monolayers on glass. *J. Colloid Interface Sci.* **2009**, 332, 432-438.

45. Vega, M. M.; Bonifacio, A.; Lughi, V.; Marsi, S.; Carrato, S.; Sergo, V. Long-term stability of surfactant-free gold nanostars. *J. Nanopart. Res.* **2014**, 16, 2729.

46. Malicka, J.; Gryczynski, I.; Gryczynski, Z.; Lakowicz, J. R. Effects of fluorophore-to-silver distance on the emission of cyanine-dye-labeled oligonucleotides. *Anal. Biochem.* **2003**, 315, 57-66.

47. Wahl, M.; Rahn, H.-J.; Gregor, I.; Erdmann, R.; Enderlein, J. Dead-time optimized time-correlated photon counting instrument with synchronized, independent timing channels. *Rev. Sci. Instrum.* **2007**, 78, 033106.

48. Taflove, A.; Hagness, S. C. *Computational Electrodynamics: the FDTD method. 3rd ed.*; Artech House: Norwood, MA, 2005.

49. Rakić, A. D.; Djurišić, A. B.; Elazar, J. M.; Majewski, M. L. Optical properties of metallic films for vertical-cavity optoelectronic devices. *Appl. Opt.* **1998**, 37, 5271-5283.

50. Oskooi, A. F.; Roundy, D.; Ibanescu, M.; Bermel, P.; Joannopoulos, J. D.; Johnson, S. G. Meep: A flexible free-software package for electromagnetic simulations by the FDTD method. *Comput. Phys. Commun.* **2010**, 181, 687-702.

51. Wang, H.; Brandl, D. W.; Nordlander, P.; Halas, N. J. Plasmonic nanostructures: artificial molecules. *Acc. Chem. Res.* **2007**, 40, 53-62.

52. Pallavicini, P.; Dona, A.; Taglietti, A.; Minzioni, P.; Patrini, M.; Dacarro, G.; Chirico, G.; Sironi, L.; Bloise, N.; Visai, L.; Scarabelli, L. Self-assembled monolayers of gold nanostars: a convenient tool for near-IR photothermal biofilm eradication. *Chem. Commun.* **2014**, 50, 1969-1971.

53. Pallavicini, P.; Taglietti, A.; Dacarro, G.; Antonio Diaz-Fernandez, Y.; Galli, M.; Grisoli, P.; Patrini, M.; Santucci De Magistris, G.; Zanoni, R. Self-assembled monolayers of silver nanoparticles

firmly grafted on glass surfaces: Low Ag+ release for an efficient antibacterial activity. *J. Colloid Interface Sci.* **2010**, 350, 110-116.

54. Nuzzo, R. G.; Dubois, L. H.; Allara, D. L. Fundamental studies of microscopic wetting on organic surfaces. 1. Formation and structural characterization of a self-consistent series of polyfunctional organic monolayers. *J. Am. Chem. Soc.* **1990**, 112, 558-569.

55. Gustafson, T. P.; Cao, Q.; Wang, S. T.; Berezin, M. Y. Design of irreversible optical nanothermometers for thermal ablations. *Chem. Commun.* **2013**, 49, 680-682.

56. Borzenkov, M.; Chirico, G.; D'Alfonso, L.; Sironi, L.; Collini, M.; Cabrini, E.; Dacarro, G.; Milanese, C.; Pallavicini, P.; Taglietti, A.; Bernhard, C.; Denat, F. Thermal and Chemical Stability of Thiol Bonding on Gold Nanostars. *Langmuir* **2015**, 31, 8081-8091.

57. Pallavicini, P.; Basile, S.; Chirico, G.; Dacarro, G.; D'Alfonso, L.; Dona, A.; Patrini, M.; Falqui, A.; Sironi, L.; Taglietti, A. Monolayers of gold nanostars with two near-IR LSPRs capable of additive photothermal response. *Chem. Commun.* **2015**, 51, 12928-12930.

58. Mayer, K. M.; Hafner, J. H. Localized Surface Plasmon Resonance Sensors. *Chem. Rev.* **2011**, 111, 3828-3857.

59. Solís, D. M.; Taboada, J. M.; Obelleiro, F.; Liz-Marzán, L. M.; García de Abajo, F. J. Optimization of Nanoparticle-Based SERS Substrates through Large-Scale Realistic Simulations. *ACS Photonics* **2017**, 4, 329-337.

60. Panchuk-Voloshina, N.; Haugland, R. P.; Bishop-Stewart, J.; Bhalgat, M. K.; Millard, P. J.; Mao, F.; Leung, W.-Y.; Haugland, R. P. Alexa Dyes, a Series of New Fluorescent Dyes that Yield Exceptionally Bright, Photostable Conjugates. *J. Histochem. Cytochem.* **1999**, 47, 1179-1188.

61. Fluorescence Quantum Yields (QY) and Lifetimes (τ) for Alexa Fluor Dyes—Table 1.5. http://www.invitrogen.com/site/us/en/home/References/Molecular-Probes-The-Handbook/tables/Fluorescence-quantum-yields-and-lifetimes-for-Alexa-Fluor-dyes.html.

62. Larsson, E. M.; Alegret, J.; Käll, M.; Sutherland, D. S. Sensing Characteristics of NIR Localized Surface Plasmon Resonances in Gold Nanorings for Application as Ultrasensitive Biosensors. *Nano Lett.* **2007**, 7, 1256-1263.

63. Centeno, A.; Alford, N.; Xie, F. Predicting the fluorescent enhancement rate by gold and silver nanospheres using finite-difference time-domain analysis. *IET Nanobiotechnol.* **2013**, 7, 50-58.

64. Wu, K.; Zhang, J.; Fan, S.; Li, J.; Zhang, C.; Qiao, K.; Qian, L.; Han, J.; Tang, J.; Wang, S. Plasmon-enhanced fluorescence of PbS quantum dots for remote near-infrared imaging. *Chem. Commun.* **2015**, 51, 141-144.

65. Abadeer, N. S.; Brennan, M. R.; Wilson, W. L.; Murphy, C. J. Distance and Plasmon Wavelength Dependent Fluorescence of Molecules Bound to Silica-Coated Gold Nanorods. *ACS Nano* **2014**, 8, 8392-8406.

66. Bharadwaj, P.; Novotny, L. Spectral dependence of single molecule fluorescence enhancement. *Opt. Express* **2007**, 15, 14266-14274.

67. Centeno, A.; Xie, F.; Alford, N. Light absorption and field enhancement in two-dimensional arrays of closely spaced silver nanoparticles. *J. Opt. Soc. Am. B* **2011**, 28, 325-330.

68. Sanchez-Gaytan, B. L.; Swanglap, P.; Lamkin, T. J.; Hickey, R. J.; Fakhraai, Z.; Link, S.; Park, S.-J. Spiky Gold Nanoshells: Synthesis and Enhanced Scattering Properties. *J. Phys. Chem. C* **2012**, 116, 10318-10324.

69. Rodríguez-Oliveros, R.; Sánchez-Gil, J. A. Gold nanostars as thermoplasmonic nanoparticles for optical heating. *Opt. Express* **2012**, 20, 621-626.

70. Ma, W. Y.; Yang, H.; Hilton, J. P.; Lin, Q.; Liu, J. Y.; Huang, L. X.; Yao, J. A numerical investigation of the effect of vertex geometry on localized surface plasmon resonance of nanostructures. *Opt. Express* **2010**, 18, 843-853.

71. Lakowicz, J. R.; Masters, B. R. *Principles of fluorescence spectroscopy. 3rd ed.*; Springer: New York, NY, 2006.

72. Dragan, A. I.; Geddes, C. D. Metal-enhanced fluorescence: The role of quantum yield, Q0, in enhanced fluorescence. *Appl. Phys. Lett.* **2012**, 100, 093115.

73. Baginskiy, I.; Lai, T.-C.; Cheng, L.-C.; Chan, Y.-C.; Yang, K.-Y.; Liu, R.-S.; Hsiao, M.; Chen, C.-H.; Hu, S.-F.; Her, L.-J.; Tsai, D. P. Chitosan-Modified Stable Colloidal Gold Nanostars for the Photothermolysis of Cancer Cells. *J. Phys. Chem. C* **2013**, 117, 2396-2410.

74. Lee, J.; Hua, B.; Park, S.; Ha, M.; Lee, Y.; Fan, Z.; Ko, H. Tailoring surface plasmons of high-density gold nanostar assemblies on metal films for surface-enhanced Raman spectroscopy. *Nanoscale* **2014**, 6, 616-623.

75. Zhang, Y.; Hong, G.; Zhang, Y.; Chen, G.; Li, F.; Dai, H.; Wang, Q. Ag_2S Quantum Dot: A Bright and Biocompatible Fluorescent Nanoprobe in the Second Near-Infrared Window. *ACS Nano* **2012**, 6, 3695-3702.

TOC graphic

